Available online at www.eccomasproceedia.org
Eccomas Proceedia UNCECOMP (2025) 569-583

ECCOMAS
Proceedia

UNCECOMP 2025
6th ECCOMAS Thematic Conference on
Uncertainty Quantification in Computational Science and Engineering
M. Papadrakakis, V. Papadopoulos, G. Stefanou (eds.)
Rhodes Island, Greece, 15-18 June 2025

A MULTI-FIDELITY REDUCED-ORDER MODEL TO QUANTIFY AERODYNAMIC FORCES ON A VERTICAL-AXIS WIND TURBINE WITH UNCERTAIN ROTATIONAL SPEED

Fausto Dicech[1] **and Lucia Parussini**[1]

[1]Università degli Studi di Trieste, Department of Engineering and Architecture
Via Alfonso Valerio 10, Trieste, Italy
e-mail: fausto.dicech@phd.units.it, lparussini@units.it

Abstract. *Wind turbines experience various uncertainties that can impact both design and control. In particular, rotational velocity is a crucial parameter, often controlled to ensure a stable and optimal power output or to avoid turbine overspeeding. This work investigates uncertainty quantification (UQ) for a vertical-axis wind turbine (VAWT), with a focus on the Darrieus VAWT type, using a multi-fidelity (MF) non-intrusive reduced order model (ROM), parameterized on the tip-speed ratio (TSR). A 2D computational fluid dynamic (CFD) model gives the high-fidelity (HF) representation of a three-bladed Darrieus VAWT with NACA0015 airfoils. A similar model with a coarser computational mesh represents the low-fidelity (LF) one. Both allow us to study the aerodynamic forces acting on the blades at different azimuthal angles for a wide range of TSRs. However, multiple evaluations of the HF model can become excessively expensive due to high computational costs, making demanding operations such as UQ not always a feasible choice. ROMs, on the other hand, can compute HF approximations in almost real-time. However, ROMs can be burdensome due to their high off-line computational costs relative to the training phase. Multi-fidelity methods extended to ROMs aim to reduce the amount of HF data required, leveraging inexpensive LF information. The present study compares the effectiveness of a MF ROM to more classical UQ approaches, such as Polynomial Chaos Expansion (PCE) on the HF solutions, and whether it is advantageous to equivalent single-fidelity ROMs. In particular, the focus is on the effect of rotational speed uncertainty on the aerodynamic forces acting on the blades, which are pivotal for turbine performances. Moreover, evaluating a ROM multiple times enables slow-convergence methods, such as Monte Carlo, with minimal effort. The MF ROM showed good UQ performance when compared to an equivalent single-fidelity ROM, especially for the mean estimates, closing the gap with a 4^{th} degree PCE in the proposed use-case.*

Keywords: Multi-fidelit , U ncertainty Q uantification Re duced Or der Mo dels, Ve rtical Axis Wind Turbine.

ISSN:2623-3339
Peer-review under responsibility of the organizing committee of UNCECOMP 2025.
doi: 10.7712/120225.12378.21079

1 INTRODUCTION

Uncertainty quantificatio (UQ) plays an importantrole whenever there is limited knowledge about the problem of interest [1]. In general, uncertainties have an inherently stochastic nature and can originate from multiple sources, where the most common are: measurements, physical modelling of the phenomena, geometrical tolerances, or computational approximations.

Many uncertainties affect wind turbines, both in their design process and control. Different approaches have been used to study UQ for wind turbines [2, 3]. Few studies used surrogate models, such as non-intrusive Reduced Order Models (ROMs), to perform UQ on wind turbines, and the literature is especially lacking for what concerns vertical axis wind turbines (VAWTs). Most of the works use ROMs only to approximate some of the VAWTs fl w features [4, 5], such as the fl w around an airfoil or the wake, but they never consider UQ problems.

In this work we want to assess the UQ capabilities of a three-bladed Darrieus VAWT multi-fidelit (MF) ROM [6]. In particular, we aim to study the uncertainty introduced by the rotational velocity on the aerodynamic forces acting on the turbine blades during an entire revolution. Rotational velocity is a crucial control parameter for VAWTs, and wind turbines in general, since it ensures a stable and optimal power output, preventing the turbine from over-speeding and ensuring grid system compatibility [7, 8]. VAWT control can be achieved in different ways, such as through blade pitch control, mechanical brakes, electric dump loads, or variable rotor resistance [9, 10, 11]. The thrust force component is the sole contributor to the shaft's torque, making it responsible for the entire VAWT power generation, and it is affected by rotational speed. As a consequence, power output can vary and fluctuat due to uncertainties in the rotational speed.

This work utilizes a non-intrusive ROM to predict the forces acting on a Darrieus VAWT's blades with a parametric tip-speed ratio (TSR). Non-intrusive ROMs [12, 13] are used in many fields such as optimization and various engineering applications, to approximate distributed outputs of numerical models, such as solution field of computational flui dynamics (CFD) problems or any vectorized quantity. Here, they enable almost real-time multiple observations of different configuration for the three-bladed Darrieus VAWT. This allows to perform effortless UQ on the uncertain input parameter. The ROM has been trained with the results of 2D transient CFD simulations of the VAWT fl w, in particular the force profile obtained during an entire turbine revolution. Since ROMs have significan offlin computational costs due to CFD simulations, MF techniques aim to improve the accuracy of the ROM while limiting the cost. Indeed, MF models leverage inexpensive and abundant low-fidelit (LF) information, i.e. coarse grid simulations, to enhance the high-fidelit (HF) problem understanding, by learning the relationship between LF and HF data.

The paper is organized as follows. Section 2 discusses the proposed methodology, Section 3 presents the use-case and analyses the results, finall Section 4 outlines the conclusions and suggest future developments.

2 METHODOLOGY

In Section 2 the methodology used will be presented, starting from what ROMs are in Section 2.1 and how their MF extension is obtained. Successi vely, in Section 2.2 the UQ will be

discussed more in depth.

2.1 Parametrized reduced order models

Traditionally, a ROM aims to approximate the solution of a set of parametrized partial differential equations (PDEs), such as in CFD problems. Even though ROMs are not as accurate as the full order model (FOM) used to solve the PDE problem, the predictions for any given parameter combination can be obtained in almost real-time. Usually, ROMs are categorized as intrusive and non-intrusive ROMs. The former are more accurate, but they are not always a feasible solution, as they require access to the FOM source code. The latter assume that the FOM is a black-box, requiring only FOM solutions for some parameter configuration during training. In this work, we focus on the non-intrusive formulation.

2.1.1 Non-intrusive reduced order models

Let's have a set of snapshots, i.e. the FOM solution fields $\mathbf{S} = \{\mathbf{u}_1(\boldsymbol{\mu}_1), ..., \mathbf{u}_n(\boldsymbol{\mu}_n)\}$ with $\mathbf{u}_i \in \mathbb{R}^N$ and $\boldsymbol{\mu}_i \in \mathbb{R}^d$ for $i = 1, ..., n$, where N is the snapshot dimension, n is the number of training snapshots, $\boldsymbol{\mu}$ is the input parameter and d is the input parameter space dimension. By applying proper orthogonal decomposition (POD) [14, 15] on the snapshot matrix $\mathbf{S}$, a set $\boldsymbol{\Phi} = \{\boldsymbol{\varphi}_1, ..., \boldsymbol{\varphi}_n\}$ of orthogonal basis function in $\mathbb{R}^N$ can be obtained, so that

$$\mathbf{S}\mathbf{S}^T\boldsymbol{\varphi}_j = \lambda_j^2\boldsymbol{\varphi}_j \quad \forall j \in 1, ..., n \tag{1}$$

where $\boldsymbol{\varphi}$ is a basis function, also called POD mode, λ_j is the singular value for the j-th mode and it is assumed that $\lambda_j \geq \lambda_{j+1}\ \forall j \in 1, ..., n-1$. Eventually, it is possible to truncate the set $\boldsymbol{\Phi}$ to the r-th mode, with $r < n$, since modes associated to higher values of λ^2 carry less information.

With the basis functions is possible to obtain a reduced representation $\mathbf{a} \in \mathbb{R}^r$, with $r \ll N$, of any snapshot $\mathbf{u}(\boldsymbol{\mu})$ by projection.

$$a_j = \mathbf{u}(\boldsymbol{\mu}) \cdot \boldsymbol{\varphi}_j \quad \forall j = 1, ..., r \tag{2}$$

Therefore, for all the snapshots belonging to $\mathbf{S}$ it is possible to compute their projection $\mathbf{a}_i$ onto the reduced basis, referred to as POD coefficient

$$\mathbf{a}_i = \{a_{i,1}, ...a_{i,r}\} = \{a_1(\boldsymbol{\mu}_i), ...a_r(\boldsymbol{\mu}_i)\} \quad \forall i = 1, ..., n \tag{3}$$

and fi a regression model $\hat{a}_j(\boldsymbol{\mu})\ \forall j = 1, ..., r$ on the pairs $(\boldsymbol{\mu}_i, a_{i,j})$, with $i = 1, ..., n$, to approximate the a_j POD coefficien for any value of the input parameter $\boldsymbol{\mu}$. Since the modes span a subspace of $\mathbb{R}^N$, the ROM prediction can be computed through a linear combination of the modes and the POD coefficient models, as follows

$$\mathbf{u}(\boldsymbol{\mu}) \sim \sum_{j=1}^{r} \hat{a}_j(\boldsymbol{\mu})\boldsymbol{\varphi}_j \tag{4}$$

Any interpolation or regression model can be used to approximate the POD coefficient models in Equation 4. The most common ones are radial basis functions (RBF), Gaussian processes (GP) regression, or neural networks (NN).

2.1.2 Multi-fidelity reduced order models

The non-intrusive ROM structure can be extended to a MF approach, where two or more FOM with different levels of accuracy are used to approximate the same PDE problem. In this framework MF models replace classical single-fidelity models for the POD coefficient $\hat{a}_j(\boldsymbol{\mu})$ in Equation 4.

A MF regression model [16, 17, 18] requires at least two information sources, an HF one and a LF one. In general, HF data is more accurate but computationally expensive, while LF data is less accurate but significantly cheaper to obtain. Therefore, if LF information can be used to enhance the knowledge of the HF problem, the overall data computational cost can be reduced without sacrificing the accuracy. To apply MF to POD coefficients a LF and HF representation a_j^{LF}, a_j^{HF} of the POD coefficient $a_j \, \forall j = 1, ..., r$ is needed. There are different ways to obtain a_j^{LF}, a_j^{HF}, and for the purpose of this work we follow [6].

Firstly, we define two snapshot matrices, a LF one $\mathbf{S}^{LF} = \{\mathbf{u}_1^{LF}, ..., \mathbf{u}_{n_L}^{LF}\}$ and a HF one $\mathbf{S}^{HF} = \{\mathbf{u}_1^{HF}, ..., \mathbf{u}_{n_H}^{HF}\}$, with $n_H \ll n_L$. All the snapshots are required to have the same cardinality $\mathbf{u}^{LF}, \mathbf{u}^{HF} \in \mathbb{R}^N$ and must be consistent in terms of connectivity. Otherwise, the snapshots should be mapped on a reference discretization, such as a computational mesh or a node distribution.

Successively, as in Equation 1, the snapshots need to be encoded with POD. The best results for MF ROMs are usually achieved mixing LF and HF snapshots. The matrix of snapshots $\mathbf{S}$ used in Equation 1 will be

$$\mathbf{S} = \mathbf{S}^{LF} \cup \mathbf{S}^{HF} \tag{5}$$

and the POD coefficient will be obtained for each POD mode by projecting the different fidelities snapshots separately on the mixed fidelity basis functions

$$a_{i,j}^{HF} = \mathbf{u}_i^{HF} \cdot \boldsymbol{\varphi}_j \quad \forall i = 1, ..., n_H \; \forall j = 1, ..., r \tag{6}$$

$$a_{k,j}^{LF} = \mathbf{u}_k^{LF} \cdot \boldsymbol{\varphi}_j \quad \forall i = 1, ..., n_L \; \forall j = 1, ..., r \tag{7}$$

Given the HF and LF POD coefficients $a_{i,j}^{HF}, a_{k,j}^{LF}$, corresponding to the training snapshots, a MF regression model can be trained for each mode. In this work, the Non-linear AutoRegressive multi-fidelity GP (NARGP) regression model [18] was chosen for its flexibility in capturing non-linear correlation patterns between fidelities

An expected improvement of a MF ROM over single-fidelity one is to achieve more accurate predictions given the same number of HF snapshots. This is obtained through the combination of the POD basis $\boldsymbol{\varphi}$ obtained mixing snapshots from different fidelities,allowing for better representation of unseen HF snapshots, and the greater NARGP accuracy when approximating the POD coefficients For further details on MF ROMs in general, as well as the specific methodology used in this work, we refer the interested reader to [6].

2.2 Uncertainty quantification

2.2.1 Polynomial Chaos Expansion

Orthogonal polynomials are used as a basis to approximate the functional form between the stochastic response output and each of its random inputs. The chaos expansion for a response

Y takes the form

$$Y(\xi) \cong \sum_{j=0}^{\infty} \alpha_j \psi_j(\xi) \tag{8}$$

with ψ_j the orthogonal polynomial of order j, α_j the chaos coefficient and ξ a random variable. From a practical standpoint, the infinite expansion is truncated at a finit expansion order, leading to

$$Y(\xi) \cong \sum_{j=0}^{P} \alpha_j \psi_j(\xi) \tag{9}$$

PCE includes a complete basis of polynomials up to a fi ed total-order specification and in this case the total number of terms N_t, in an expansion of total order p involving n random variables is given by

$$N_t = 1 + P = 1 + \sum_{s=1}^{p} \frac{1}{s!} \prod_{r=0}^{s-1} (n+r) = \frac{(n+p)!}{n!p!} \tag{10}$$

Stochastic Collocation technique [19] can be used to determine α_j coefficient with $j = 0, ..., P$. Once the chaos coefficient are known, a direct estimation of the systems' statistics can be done. The mean $\mathbb{E}[Y(\xi)]$ is analytically computed as

$$\mathbb{E}[Y(\xi)] \sim \sum_{j=0}^{P} \alpha_j \langle \psi_j(\xi) \rangle = \alpha_0 \tag{11}$$

and the variance σ_Y^2 as

$$\sigma_Y^2 = \mathbb{E}[Y(\xi)^2] - \mathbb{E}[Y(\xi)]^2 \sim \sum_{i=0}^{P} \sum_{j=0}^{P} \alpha_i \alpha_j \langle \psi_i(\xi) \psi_j(\xi) \rangle - \alpha_0^2 = \sum_{j=1}^{P} \alpha_j^2 \left\langle \psi_j^2(\xi) \right\rangle \tag{12}$$

where $\mathbb{E}[\cdot]$ is the expected value. In this work, ξ follows a Gaussian distribution, therefore the appropriate orthogonal polynomial ψ_j choice for the expansion is the Hermite polynomials.

2.2.2 Monte Carlo

Classical Monte Carlo (MC) methods for UQ are used for uncertainty propagation [20]. If the model's input parameter uncertainties are represented by a random variable ξ, a MC method aims to approximate the stochastic response output Y of the model. Indeed, to approximate the expected value $\mathbb{E}[Y(\xi)]$, MC methods requires to sample M times the ξ random variable and compute as many deterministic responses from the model $y_1, ..., y_M$. The $\mathbb{E}[Y(\xi)]$ is approximated with the average of the outputs, as in

$$\mathbb{E}[Y(\xi)] \sim \bar{y} = \frac{1}{M}\sum_{i=1}^{M} y_i \tag{13}$$

and the variance σ_Y^2 can be estimated as well, as

$$\sigma_Y^2 = \mathbb{E}[Y(\xi)^2] - \mathbb{E}[Y(\xi)]^2 \sim \frac{1}{M}\sum_{i=1}^{M}(y_i - \bar{y})^2 \tag{14}$$

Due to the strong law of large numbers, $\bar{y}$ should converge to the actual expected value $\mathbb{E}[Y(\xi)]$ with enough samples M. However, the convergence rate is rather slow, being $\mathcal{O}(\sqrt{M})$.

3 RESULTS

In Section 3 the results will be presented, starting from the case-study description in 3.1 and then moving to the actual results analysis in Section 3.2

3.1 Problem description

In this work the force profile during an entire revolution of a VAWT are studied under rotational speed uncertainty. In particular, the considered turbine is a Darrieus three-bladed VAWT with NACA0015 profiles each with a chord length of 420 mm, as in [21]. The CFD simulations simplify the problems to be two-dimensional, with a constant wind speed $U = 10$ m/s. The rotational speed of the turbine is the only control parameter, ensuring values of the TSR $\lambda \in [0.9, 1.32]$, define in Equation 15.

$$\lambda = \frac{\omega R}{U} \tag{15}$$

where R is the radius between the turbine blade and the center of rotation, and ω is the rotational speed. Instead of approximating CFD solution field on the spatial discretization, the ROM will be utilized to surrogate the thrust force F_T acting on a blade, as shown in Figure 1, on the time discretization. Specificall , the time values will be matched with their corresponding azimuthal angle θ discretization.

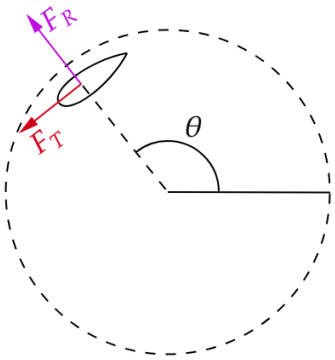

Figure 1: Thurst and radial forces F_T, F_R components acting on a VAWT blade at an angle θ.

This work will focus mainly on the F_T component, since it is the sole contributor to the power generation and it is more relevant for this type of application. The radial component F_R remains crucial from a structural design perspective. Figure 2 shows examples of force profile obtained from simulations at different λ and will be used as snapshots for the ROMs.

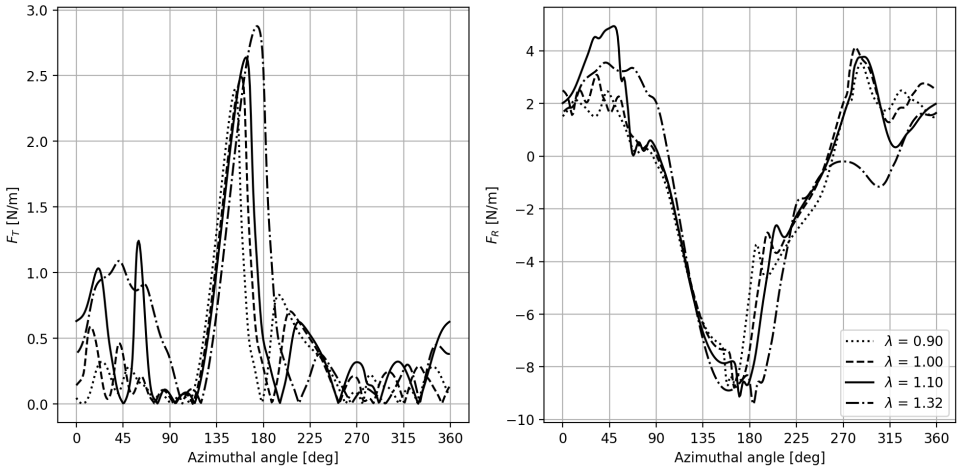

Figure 2: Thurst (left) and radial (right) forces components during an entire revolution for different values of λ.

3.1.1 Simulation set-up

The computation has been carried out with Ansys Fluent, solving for the transient RANS equations alongside the $k\omega$-SST turbulence model. The blades rotation was modelled with a cylindrical sliding mesh centred on the rotational axis of the VAWT. Figure 3 shows a schematic representation of the domain. Many works discuss in detail the best procedures and reccommendations to set-up a 2D VAWT CFD simulation [22].

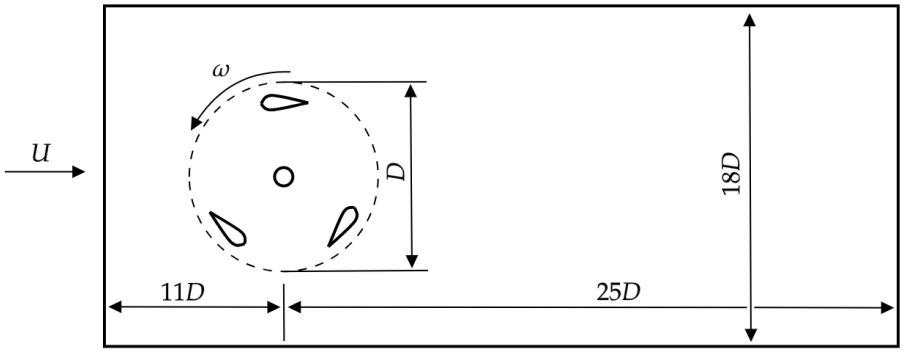

Figure 3: Schematics of the 2D CFD domain. $D = 2.8$ m here represents the diameter of the rotating mesh region.

The LF and HF solutions differ in their computational mesh granularity, where the LF grid is coarser, with 107k cells, while the HF one has 411k cells, as Figure 4 shows. Time discretization depends solely on ω, ensuring a rotation of 1° per time-step in both LF and HF simulations.

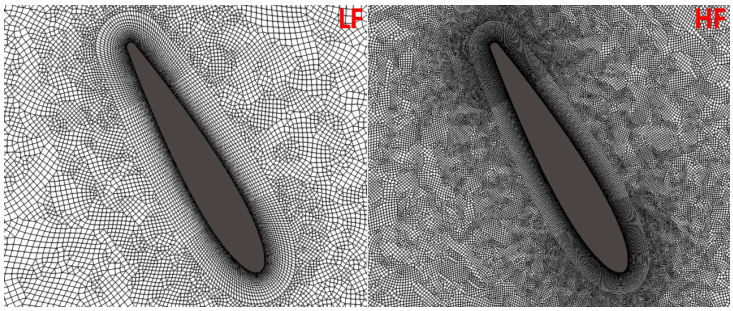

Figure 4: Close up of the computational mesh around one blade for a LF solution (left) and for an HF solution (right).

The HF results are reasonably consistent with the reference experimental measurements [21]. Figure 5 shows a power coefficien value comparison between the HF CFD and the experimental results. The power coefficien represents the performance of the turbine and is computed as in Equation 16. The slight CFD overestimation can be attributed to the 2D simplificatio of the problem, where the degrading effects of 3D fl w features, such as tip vortices or the flui interaction with the support structures, cannot be modelled.

$$C_P = \frac{P_t}{P_w} = \frac{\omega R N_b \frac{1}{2\pi} \int_0^{2\pi} F_T(\theta) d\theta}{\frac{1}{2}\rho U^3 2RH} \tag{16}$$

where P_t is the turbine power, P_w is the wind power, N_b is the number of blades, F_T is the thrust component of the aerodynamic force acting on a single blade, θ is the azimuthal angle of the blade, ρ is the air density and H is the height of the wind turbine's swept area.

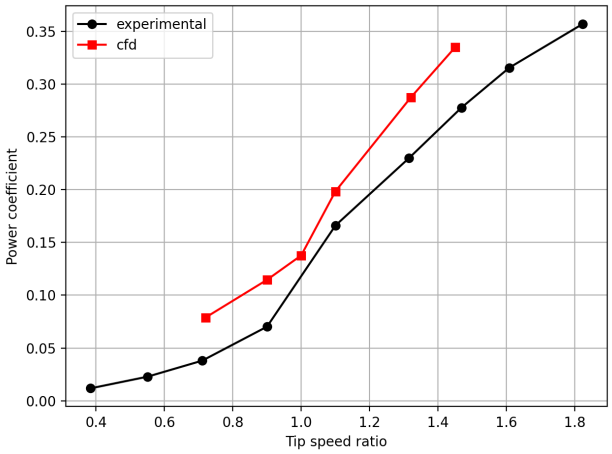

Figure 5: Power coefficien measurements from [21] vs current work HF CFD results.

3.1.2 Uncertain variable

As previously mentioned, in this work we consider the rotational speed ω to be the uncertain variable. Since the wind speed U is kept constant, the TSR λ is just a scaled version of ω, and are interchangeable.

Rotational speed in wind turbines, or in any low-speed rotor in general, can be measured using different sensors and techniques, such as Hall-effect sensors, tachometers or image-processing methodologies [23, 24, 25]. For the purpose of this work, we assume an accuracy of ± 0.5 rpm for the VAWT's hypothetical rotational speed measurement. In fact, under the considered operating conditions the turbine rotates at a speed of approximately $70 - 100$ rpm, and a $0.5 - 1\%$ error is close to what has been observed in literature. Therefore, the UQ is performed under the hypothesis that ω follows a Gaussian distribution with a standard deviation $\sigma = 0.25$ rpm, having the 95% of the distribution lying within 1 rpm of the mean.

3.2 Analysis and results

Considering $\lambda = 1.25$, or alternatively $\omega = 85.3$ rpm, we want to compare a 4^{th} degree PCE mean and second order statistical moment estimates to the ones obtained with a MC simulation performed with single- and multi- fidel ty ROMs. The 4^{th} degree PCE will be used as the ground truth throughout this work.

Table 1 presents the HF solutions computed for the ROM design of experiment (DoE) and for the PCE.

Tip-speed ratio	Use-case
0.9	ROM
0.95	ROM
1.0	ROM
1.1	ROM
1.15	ROM
1.2	ROM
1.225	ROM
1.23953	PCE 4^{th} deg
1.24365	PCE 2^{nd} deg
1.24503	PCE 4^{th} deg
1.25	PCE $2^{nd}/4^{th}$ deg
1.25497	PCE 4^{th} deg
1.25635	PCE 2^{nd} deg
1.26047	PCE 4^{th} deg
1.32	ROM

Table 1: Input parameter locations for the HF utilized for the ROMs and the PCE.

Figure 6 shows the differences between a 2^{th} and 4^{th} degree PCE for the thrust force. The mean estimate error is $E = 1.2\%$, while the second order moment tends to be underestimated by the 2^{nd} degree PCE. Equation 17 shows how the error metric is evaluated

$$E = \frac{\|\mathbb{E}[\mathbf{u}_{pred}] - \mathbb{E}[\mathbf{u}_{true}]\|_2}{\|\mathbb{E}[\mathbf{u}_{true}]\|_2} \tag{17}$$

where $\|\cdot\|_2$ is the l^2-norm, $\mathbb{E}[\mathbf{u}_{true}]$ is the ground truth mean estimate, i.e. the 4^{th} degree PCE, and $\mathbb{E}[\mathbf{u}_{pred}]$ is the estimate obtained with the compared model.

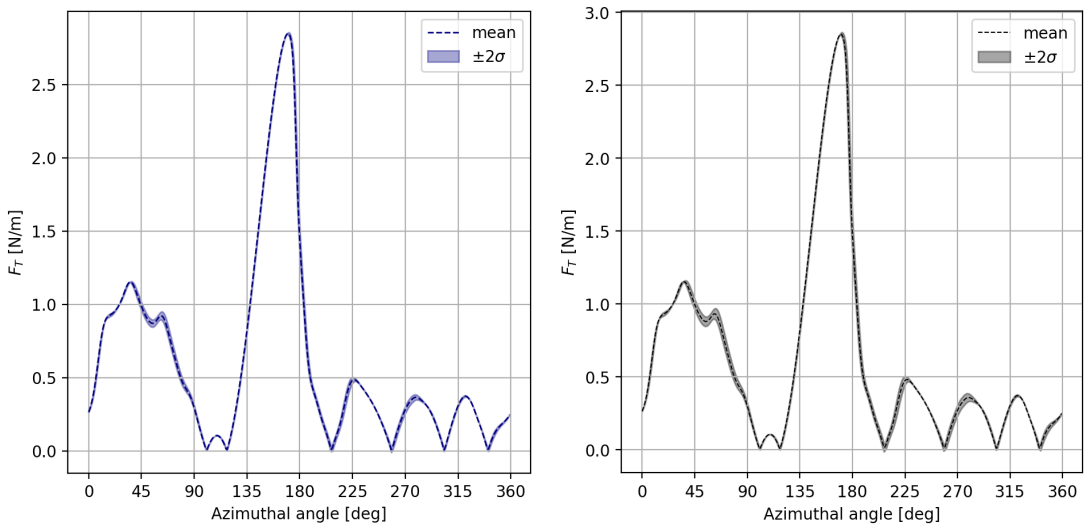

(a) 2^{nd} degree PCE.

(b) 4^{th} degree PCE.

Figure 6: First and second order moment estimates of F_T with PCE.

A single-fidelit HF ROM and a MF ROM can be used to perform a MC simulation and estimate the statistical moments for F_T. According to Section 2.1.1, the HF ROM was trained using GP regression models to approximate the POD coefficients A total of 8 HF snapshots were used, as in Table 1. The same 8 HF snapshots were considered for the MF model together with 23 LF snapshots, evenly distributed in $\lambda \in [0.9, 1.32]$, with an approximate computational cost ratio of $5 : 1$ when compared to HF simulations. Figure 7 shows the estimates of 3000 thousands MC simulations obtained with the HF ROM and the MF ROM.

The MF ROM mean estimate is more accurate than the HF ROM one, suggesting that the addition of LF snapshots is benefi ial to the ROM training. Table 2 shows the two ROMs mean estimates errors with respect to the 4^{th} degree PCE, with the MF ROM having a better accuracy than the HF ROM.

	HF ROM	MF ROM
E	6.8%	2.9%
wall time [s]	0.0255	21.6

Table 2: ROMs MC simulation mean estimates error compared to ground truth, i.e. 4^{th} degree PCE, and wall time with a Intel Core i7-1255U CPU.

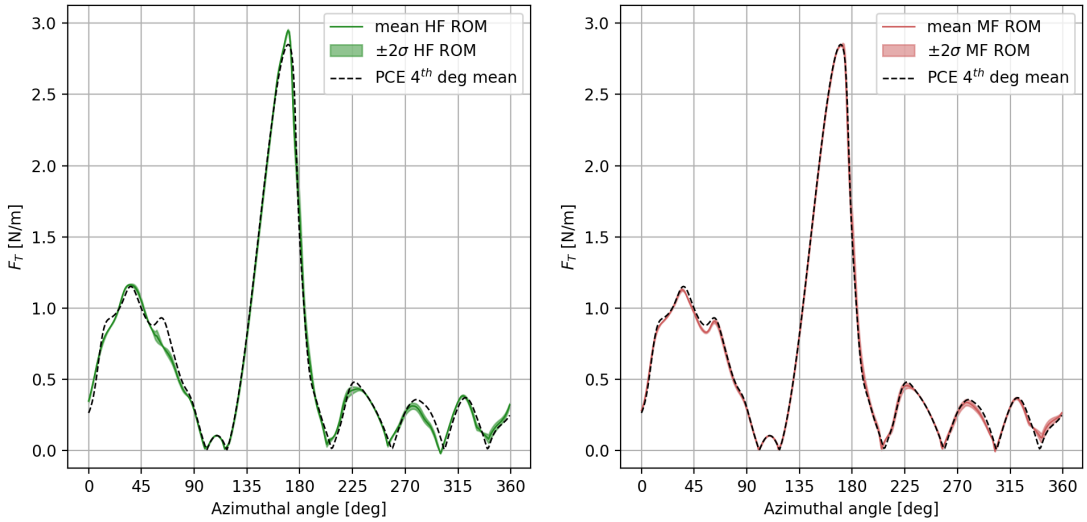

(a) Single-fidelit HF ROM. (b) MF ROM.

Figure 7: First and second order moment MC estimates of F_T ROMs compared to 4^{th} degree PCE.

The errors on the mean estimates presented in Table 2 are aligned with the reconstruction error of both ROMs. The ROM reconstruction error E_r measures the ROM accuracy when approximating an unseen HF snapshot, and is computed as

$$E_r = \frac{\|\mathbf{u}^{ROM} - \mathbf{u}^{HF}\|_2}{\|\mathbf{u}^{HF}\|_2} \tag{18}$$

where $\mathbf{u}^{ROM}$ is the ROM approximation of the HF snapshot $\mathbf{u}^{HF}$. If the HF ROM and MF ROM are used to predict the F_T in the 7 λ locations associated with the 2^{nd} and 4^{th} degree PCE snapshots of Table 1, the mean reconstruction error for the two models are respectively of 6.7% and 2.8%. If the corresponding 7 LF snapshots were used as they are instead of the ROM approximations in Equation 18, the discrepancy between the LF and the HF snapshots would be 19.7%. This highlights that LF information is inaccurate and it is not suitable for studying the HF problem by itself, but it can significantl improve the MF ROM performances.

Figure 8 shows that the ROMs are able to identify the locations with high variances. However, both ROMs underestimate the PCE second order moment estimates

According to Equation 16, it is possible to integrate the F_T realizations obtained with the HF ROM and the MF ROM MC simulations, each corresponding to a different ω, and fin the turbine power coefficien C_P. Similarly, the F_T PCE mean estimate can be used as well to compute the C_P for a ω corresponding to $\lambda = 1.25$.

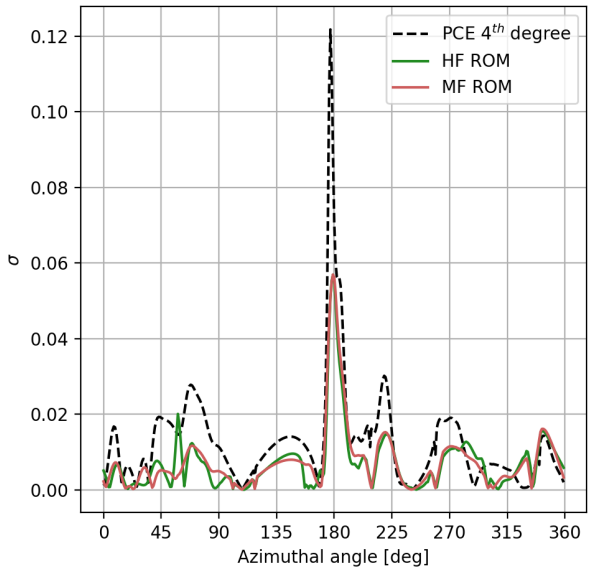

Figure 8: Comparison between the standard deviation σ associated to the second order moment estimates of the HF ROM, the MF ROM and the PCE.

Figure 9 shows that the mean C_P obtained with the integration of MF ROM F_T predictions is very close to the one obtained with the PCE mean estimation, with a relative error of 0.51%. Again, the single-fidelit ROM is less performant, showing a 1.43% relative error when estimating the mean C_P under uncertain rotational velocity.

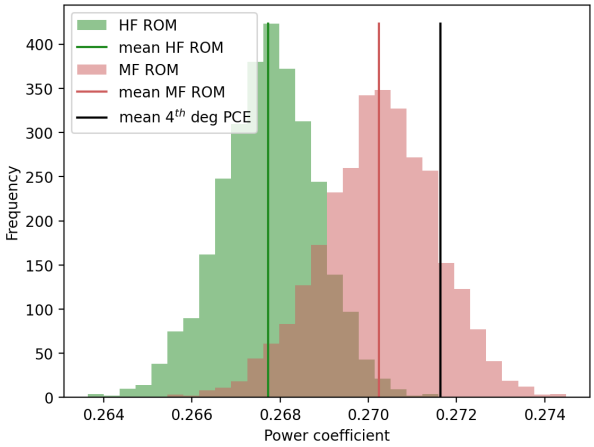

Figure 9: Comparison between the power coefficien C_P computed from HF ROM MC realizations, the MF ROM ones, and the PCE mean estimate.

4 CONCLUSIONS

This work compares a MC method applied together with a ROM against a classical PCE for the UQ of the aerodynamic forces acting on a Darrieus VAWT, under uncertain rotational velocity. In particular, a single-fidelit HF ROM and a MF ROM is proposed. Results show that the MF ROM in combination with the MC method performs similarly to a 4^{th} degree PCE, especially for the mean estimates. Moreover, the HF snapshots for the ROMs are sampled in a much wider input parameter domain than those for the PCE, resulting in an overall poor HF information density. On the other hand, a HF ROM trained on the same few HF snapshots shows higher errors than the MF ROM. This indicates that the addition of cheaper and otherwise useless LF information can be beneficia to the MF ROM. Additionally, the two ROMs reconstruction errors are in line with their MC mean error, suggesting that the ROM reconstruction error could have some potential as an empirical error estimator for UQ. Both HF ROM and MF ROM, however, underestimate the second order statistical moment. Finally, the MF ROM higher accuracy is again confirme when considering the power coefficien mean estimates.

Future work will focus on extending the approach to a more complex parameterization to further understand MF ROM capabilities for UQ.

REFERENCES

[1] Cinnella, P., Congedo, P., Parussini, L. & Pediroda, V. Quantificatio of thermodynamic uncertainties in real gas fl ws. *International Journal Of Engineering Systems Modelling And Simulation*. **2**, 12-24 (2010) doi: 10.1504/IJESMS.2010.031867 .

[2] Santiago, A., Alonso, J., Palacios, F., Barone, M. & Eldred, M. Multi-Fidelity Uncertainty Quantification Application to a Vertical Axis Wind Turbine Under an Extreme Gust. *AIAA AVIATION 2014 -15th AIAA/ISSMO Multidisciplinary Analysis And Optimization Conference*. (2014,6) doi: 10.2514/6.2014-3013 .

[3] Bortolotti, P., Canet, H., Bottasso, C. & Loganathan, J. Performance of non-intrusive uncertainty quantific tion in the aeroservoelastic simulation of wind turbines. *Wind Energy Science*. **4**, 397-406 (2019) doi: 10.5194/wes-4-397-2019 .

[4] Tabib, M., Tsiolakis, V., Pawar, S., Ahmed, S., Rasheed, A., Kvamsdal, T. & San, O. Hybrid deep-learning POD-based parametric reduced order model for fl w around wind-turbine blade. *Journal Of Physics: Conference Series*. **2362**, 012039 (2022,11) doi: 10.1088/1742-6596/2362/1/012039 .

[5] Luo, Z., Wang, L., Xu, J., Wang, Z., Yuan, J. & Tan, A. A reduced order modeling-based machine learning approach for wind turbine wake fl w estimation from sparse sensor measurements. *Energy*. **294** pp. 130772 (2024) doi: 10.1016/j.energy.2024.130772 .

[6] Dicech, F., Gkaragkounis, K., Parussini, L., Spagnolo, A. & Telib, H. Integration of multi-fidelit methods in parametrized non-intrusive reduced order models for industrial applications. *Journal Of Computational Science*. **85** pp. 102511 (2025) doi: 10.1016/j.jocs.2024.102511 .

[7] Mihet-Popa, L., Blaabjerg, F. & Boldea, I. Wind Turbine Generator Modeling and Simulation Where Rotational Speed is the Controlled Variable. *Industry Applications, IEEE Transactions On*. **40** pp. 3 - 10 (2004,2) doi: 10.1109/TIA.2003.821810 .

[8] Sadman Sakib, M., Todd Griffith D., Hossain, S., Bayat, S. & Allison, J. Intracycle RPM control for vertical axis wind turbines. *Wind Energy*. **27**, 202-224 (2024) doi: 10.1002/we.2885 .

[9] Burnham, D., Santoso, S. & Muljadi, E. Variable rotor-resistance control of wind turbine generators. *2009 IEEE Power & Energy Society General Meeting*. pp. 1-6 (2009) doi: 10.1109/PES.2009.5275637 .

[10] Yamada, T., Kiwata, T., Kita, T., Hirai, M., Komatsu, N. & Kono, T. Overspeed Control of a Variable-Pitch Vertical-Axis Wind Turbine by Means of Tail Vanes. *Journal Of Environment And Engineering*. **7**, 39-52 (2012) doi: doi.org/10.1299/jee.7.39 .

[11] Pinar Pérez, J., García Márquez, F., Tobias, A. & Papaelias, M. Wind turbine reliability analysis. *Renewable And Sustainable Energy Reviews*. **23** pp. 463-472 (2013) doi: 10.1016/j.rser.2013.03.018 .

[12] Hesthaven, J. & Ubbiali, S. Non-intrusive reduced order modeling of nonlinear problems using neural networks. *Journal Of Computational Physics*. **363** pp. 55-78 (2018), doi: 10.1016/j.jcp.2018.02.037 .

[13] Scardigli, A., Arpa, R., Chiarini, A. & Telib, H. Enabling of Large Scale Aerodynamic Shape Optimization Through POD-Based Reduced-Order Modeling and Free Form Deformation. *Computational Methods In Applied Sciences*. **48** pp. 49 - 63 (2019) doi: 10.1007/978-3-319-89988-6 _4 .

[14] Benner, P., Gugercin, S. & Willcox, K. A Survey of Projection-Based Model Reduction Methods for Parametric Dynamical Systems. *SIAM Review*, **57** pp. 483-531 (2015) doi: 10.1137/130932715 .

[15] Sirovich, L. Turbulence and the dynamics of coherent structures. Part I, II and III. *Quarterly of Applied Mathematics* **45** pp. 561-571 (1987) doi: 10.1090/qam/910462 .

[16] Kennedy, M. & O'Hagan, A. Predicting the output from a complex computer code when fast approximations are available. *Biometrika*. **87**, 1-13 (2000) doi: 10.1093/biomet/87.1.1 .

[17] Le Gratiet, L. & Garnier, J. Recursive co-kriging model for design of computer experiments with multiple levels of fidelit . *Int J Uncertain Quantif*. **4**, 365-386 (2014) doi: 10.1615/int.j.uncertaintyquantification.201400691 .

[18] Perdikaris, P., Raissi, M., Damianou, A., Lawrence, N. & Karniadakis, G. Nonlinear information fusion algorithms for data-efficien multi-fidelit modelling. *Proceedings Of The Royal Society A: Mathematical, Physical And Engineering Sciences*. **473** (2017) doi: 10.1098/rspa.2016.0751 .

[19] Xiu, D. Numerical Methods for Stochastic Computations: A Spectral Method Approach. *Princeton University Press*. (2010) doi: 10.2307/j.ctv7h0skv .

[20] Zhang, J. Modern Monte Carlo methods for efficien uncertainty quantificatio and propagation: A survey. *WIREs Computational Statistics*. **13**, e1539 (2021) doi: 10.1002/wics.1539 .

[21] McLaren, K. A numerical and experimental study of unsteady loading of high solidity vertical axis wind turbines. (McMaster University,2011), url: http://hdl.handle.net/11375/11096.

[22] Balduzzi, F., Bianchini, A., Maleci, R., Ferrara, G. & Ferrari, L. Critical issues in the CFD simulation of Darrieus wind turbines. *Renewable Energy*. **85** pp. 419-435 (2016) doi: 10.1016/j.renene.2015.06.048 .

[23] Liao, Y., Wang, L. & Yan, Y. Instantaneous Rotational Speed Measurement of Wind Turbine Blades using a Marker-Tracking Method. *2022 IEEE International Instrumentation And Measurement Technology Conference (I2MTC)*. pp. 1-5 (2022) doi: 10.1109/I2MTC48687.2022.9806658 .

[24] Wang, Y., Wang, L. & Yan, Y. Rotational speed measurement through digital imaging and image processing. *2017 IEEE International Instrumentation And Measurement Technology Conference (I2MTC)*. pp. 1-6 (2017) doi: 10.1109/I2MTC.2017.7969697 .

[25] Rapos, D., Mechefske, C. & Timusk, M. Dynamic sensor calibration: A comparative study of a Hall effect sensor and an incremental encoder for measuring shaft rotational position. *2016 IEEE International Conference On Prognostics And Health Management (ICPHM)*. pp. 1-5 (2016) doi: 10.1109/ICPHM.2016.7542858 .